

points and precise stable manifolds in the original system dynamic. The advantage to our approach is that once a transition to rhythmicity is predicted, the initiation of a control action may begin immediately without a lengthy learning stage during the seizure activity. In addition, being able to predict state transitions of a dynamical system allows for successful control actions using only small perturbations to the state variables. The approach of Schiff *et al.* has the advantage of learning the less complex dynamics which could be a considerably easier task than learning the higher complexity dynamics. Reported chaos control strategies such as those in [9] require constant stimulation until the state point was on a two dimensional fixed point. Alternatively, our design only required a small perturbation on the system variable when the system dynamic is sufficiently close to the higher complexity manifold. While the efforts to maintain chaos in the neuronal tissue was usually limited to eliciting action potentials to modify the interspike interval patterns, our approach utilizes the intrinsic vector fields of the system so that only small perturbations are required.

## VII. CONCLUSION

We have developed an approach to a possible therapy for epileptic seizures. Whenever state transitions into rhythmicity are predicted, the control strategy uses the ANN to provide a sufficiently small electrical perturbation to the system such that the variable will be attracted to the estimate of the unstable manifold of the rhythmic mode using the system's intrinsic vector fields. The underlying assumption that small perturbations induced at the correct time during state transitions can sufficiently perturb the system onto the unstable manifold was demonstrated. Furthermore, this has the effect of restoring the system to its higher complexity mode regardless of the original nature of the system dynamics.

## ACKNOWLEDGMENT

The authors would also like to thank A. Courville from the Robotics Institute at Carnegie Mellon for his helpful suggestions with regards to the prediction and control strategies, and T. Le for performing correlation dimension analysis on the signals.

## REFERENCES

- [1] B. L. Bardakjian and N. E. Diamant, "A mapped clock oscillator model for transmembrane electrical rhythmic activity in excitable cells," *J. Theor. Biol.*, vol. 166, pp. 225–235, 1994.
- [2] B. L. Bardakjian, R. Aschebrenner-Scheibe, J. L. Perez-Velazquez, and P. Carlen, "Transmembrane voltage oscillations in CA3 neurons," in *Proc. IEEE 17th Annu. Conf. EMBS*, vol. 17, 1995, pp. 1503–1504.
- [3] W. J. Freeman, "Tutorial on neurology: from single neurons to brain chaos," *Int. J. Bifurcation Chaos*, vol. 2, no. 3, pp. 451–482, 1992.
- [4] S. J. Schiff, K. Jerger, D. H. Duong, T. Chang, M. L. Spano, and W. L. Ditto, "Controlling chaos in the brain," *Nature*, vol. 370, pp. 615–620, 1994.
- [5] M. L. V. Quyen, J. Martinier, C. Adam, and F. J. Varela, "Unstable periodic orbits in human epileptic activity," *Phys. Rev. E*, vol. 56, pp. 3401–3411, Sept. 1997.
- [6] B. Gluckman, H. Nguyen, S. Weinstein, and S. Schiff, "Adaptive electric field control of epileptic seizures," *J. Neurosci.*, vol. 21, no. 2, pp. 590–600, 2001.
- [7] D. M. Durand and M. Bikson, "Suppression and control of epileptiform activity by electrical stimulation: a review," *Proc. IEEE*, vol. 89, pp. 1065–1082, 2001.
- [8] D. J. Christini and J. Collins, "Control of chaos in excitable physiological systems: a geometric analysis," *Chaos*, vol. 7, no. 4, pp. 544–549, 1997.
- [9] M. W. Slutzky, P. Cvitanovic, and D. J. Mogul, "Manipulating epileptiform bursting in the rat hippocampus using chaos control and adaptive techniques," *IEEE Trans. Biomed. Eng.*, vol. 50, pp. 559–570, May 2003.
- [10] A. Wolf, J. B. Swift, H. L. Swinney, and J. A. Vastano, "Determining Lyapunov exponents from a time series," *Physica D*, vol. 16, pp. 285–317, 1985.
- [11] L. D. Iasemidis, D. S. Shiau, W. Chaovalitwongse, J. C. Sackellares, P. M. Pardalos, J. C. Principe, P. R. Carney, A. Prasad, B. Veeramani, and K. Tsakalis, "Adaptive epileptic seizure prediction systems," *IEEE Trans. Biomed. Eng.*, vol. 50, pp. 616–627, May 2003.
- [12] E. Ott, C. Grebogi, and J. A. Yorke, "Controlling chaos," *Phys. Rev. Lett.*, vol. 64, no. 11, pp. 1196–1199, 1990.
- [13] D. J. Christini and J. J. Collins, "Using noise and chaos control to control nonchaotic systems," *Phys. Rev. E*, vol. 52, pp. 5806–5809, 1995.
- [14] —, "Using chaos control and tracking to suppress a pathological nonchaotic rhythm in a cardiac model," *Phys. Rev. E*, vol. 53, pp. 49–52, 1996.
- [15] A. Courville and B. L. Bardakjian, "Chaosmakers: rhythmicity breakers," in *Proc. IEEE 1st Joint BMES/EMBS Conf.*, vol. 1, 1999, p. 406.

## Lesion Size Estimator of Cardiac Radiofrequency Ablation at Different Common Locations With Different Tip Temperatures

Yu-Chi Lai, Young Bin Choy, Dieter Haemmerich, Vicken R. Vorperian, and John G. Webster\*

**Abstract**—Finite element method (FEM) analysis has become a common method to analyze the lesion formation during temperature-controlled radiofrequency (RF) cardiac ablation. We present a process of FEM modeling a system including blood, myocardium, and an ablation catheter with a thermistor embedded at the tip. The simulation used a simple proportional-integral (PI) controller to control the entire process operated in temperature-controlled mode. Several factors affect the lesion size such as target temperature, blood flow rate, and application time. We simulated the time response of RF ablation at different locations by using different target temperatures. The applied sites were divided into two groups each with a different convective heat transfer coefficient. The first group was high-flow such as the atrioventricular (AV) node and the atrial aspect of the AV annulus, and the other was low-flow such as beneath the valve or inside the coronary sinus. Results showed the change of lesion depth and lesion width with time, under different conditions. We collected data for all conditions and used it to create a database. We implemented a user-interface, the lesion size estimator, where the user enters set temperature and location. Based on the database, the software estimated lesion dimensions during different applied durations. This software could be used as a first-step predictor to help the electrophysiologist choose treatment parameters.

**Index Terms**—Ablation, bio-heat equation, cardiac ablation, finite element method, RF ablation, temperature-controlled ablation.

## I. INTRODUCTION

Because of the efficacy, controllability, and minimal invasiveness, radiofrequency (RF) catheter ablation has proven an effective method to treat some cardiac arrhythmias, such as atrioventricular (AV) node

Manuscript received August 9, 2003; revised February 22, 2003. This work was supported by the National Institute of Health (NIH) under Grant HL56413. Asterisk indicates corresponding author.

Y.-C. Lai is with the Department of Electrical and Computer Engineering, University of Wisconsin, Madison, WI 53706 USA.

Y. B. Choy is with the Department of Electrical and Computer Engineering, University of Illinois, Urbana, IL 61801 USA.

D. Haemmerich is with the Department of Surgery, University of Wisconsin, Madison, WI 53792 USA.

V. R. Vorperian is with the Department of Medicine, University of Wisconsin, Madison, WI 53792 USA.

\*J. G. Webster is with the Department of Biomedical Engineering, University of Wisconsin, 1550 Engineering Drive, Madison, WI 53706 USA (e-mail webster@engr.wisc.edu).

Digital Object Identifier 10.1109/TBME.2004.831529

re-entry, atrial tachycardia, atrial flutter, and fascicular ventricular tachycardias [1]–[3]. Several research groups also suggested that it may be a good method for palliative suppression of ventricular tachycardias [3]–[5].

In order to analyze the relationship between the set temperature in temperature-controlled mode and lesion size in the cardiac tissue during RF ablation, we solved the bioheat equation. Commercial software (ABAQUS), a common Finite element method (FEM) bioheat equation solver, was used to determine the temperature distribution in the myocardium. FEM modeling takes into account myocardial properties (electrical conductivity, thermal conductivity, density, and specific heat capacity) and the convection of the blood flow. Thus, it has been demonstrated that it is a useful tool in qualitative assessment of lesion dimensions created by RF ablation [6]–[8]. Early simulations such as Tungjikusolmun *et al.* [8] used trial and error adjustment of the applied voltage at each time step to control the tip temperature at the set value. Haemmerich *et al.* [9] implemented a simple proportional-integral (PI) controller for hepatic ablation simulation. In this study, we adjusted the control coefficients to fit cardiac characteristics. In temperature-controlled mode, the controlled temperature was sensed from an insulated thermistor in contact with the endocardium at the tip of the catheter and fed back to the PI controller. The PI controller increased the applied power gradually and let the tip temperature approach the set value with minimum overshoot at the set temperature. This is similar to the commercial ablation generator. Thus, we expected to obtain similar temporal behavior as in the *in vivo* experiments. In addition, with the aid of the computer, we could also set the time-step shorter to make the simulation more precise.

In addition to the set temperature, the blood flow in the heart chambers also plays an important role in lesion formation during RF ablation. The blood flow carries heat away from the endocardium and from the electrode by convection. It has a cooling effect on the myocardium and has a large impact on the final lesion size [7], [10], [11]. The blood velocities are significantly different at different locations inside the heart. So the cooling effect due to blood convection differs at different ablation locations. Even though the tip temperature is set at the same temperature, different lesion sizes result at different locations.

Thus, our objective was to quantify the effect of changing ablation catheter tip temperature, in different locations in the heart chamber with different blood velocities on the FEM calculation of the lesion size as a function of the applied ablation time.

## II. METHOD

The formation of the RF ablation lesion depends on the temperature distribution inside the tissue. The temperature change during ablation inside the myocardium is governed by the bioheat equation [6]. By using the critical temperature  $50^{\circ}\text{C}$ , we determined the depth and width of the lesion. Because it was not practical to solve the coupled problem analytically, we used FEM modeling to solve it numerically.

Fig. 1 shows a simple system for the energies involved during RF ablation. The RF generator generates the electric power delivered to the system by the electrode. At the electrode-myocardium interface, the electric power is transformed to Joule heating, which increases the temperature of the tissue around the electrode. Thermal conduction causes increasing temperature deeper in the myocardium and in the thermistor at the tip of the catheter. However, blood convection in the cardiac chamber cools down the blood-contacting surface of the electrode and the myocardium. FEM simulation predicts the process of the ablation from power delivered, duration, geometry, material characteristics and myocardial properties, such as resistivity, thermal conductivity, specific heat, etc., which vary with temperature.

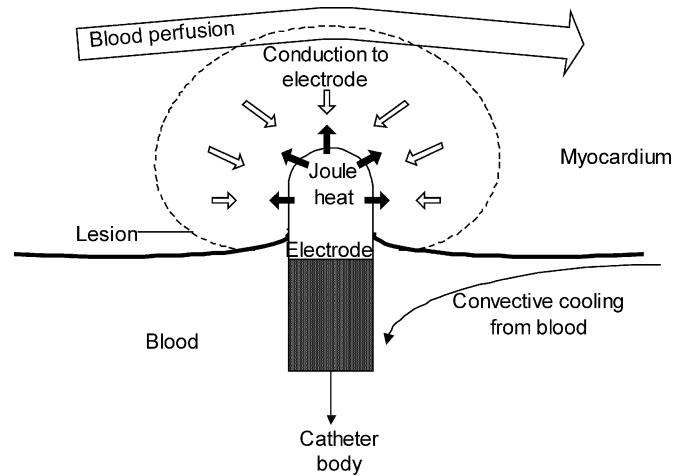


Fig. 1. Electric power through the electrode heats the myocardium. Blood velocity cools it. The black arrows represent the Joule heat generated within about the first 1 mm of myocardium. During about 30 s, the heat is conducted to the full lesion size. The white arrows represent the heat conduction back into the electrode, which has negligible self-heating.

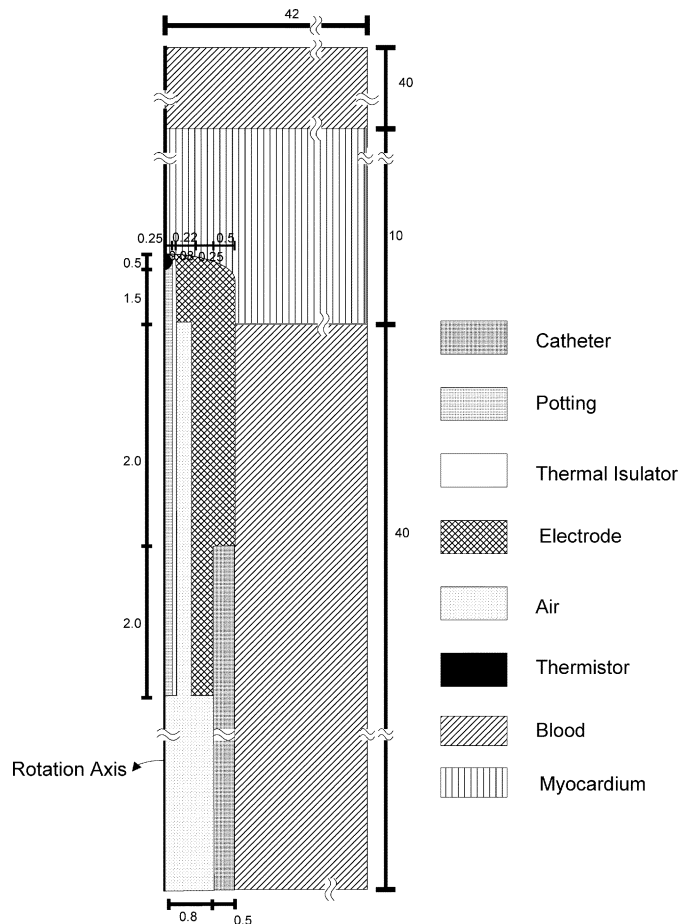


Fig. 2. The geometry of the standard size ablation electrode in millimeters.

For all of the simulations performed in this paper, the ablation electrode was of standard size used in clinical practice (4 mm long, and 2.6 mm diameter). A temperature-sensing thermistor was embedded at the electrode tip. Similar to Tungjikusolmun *et al.* [6], we modeled the system by an axisymmetric model. The catheter tip was pushed into the myocardium a distance of 2 mm. The blood pool extended 40 mm beyond the myocardium. It was used to model the body fluid beyond the myocardium. We assumed that beyond the myocardium was totally

TABLE I  
CONVECTIVE HEAT TRANSFER COEFFICIENT AND FLOW STATE IN DIFFERENT APPLIED LOCATIONS

Location	Blood flow	$h_b$ at blood-myocardium interface [W/(m <sup>2</sup> ·K)]	$h_{be}$ at blood-electrode interface [W/(m <sup>2</sup> ·K)]
AV node	High	7100	6090
CS	Low	3350	2081
Atrial AP	High	7100	6090
Ventricular AP	Low	3350	2081
RV outflow VT	High	7100	6090

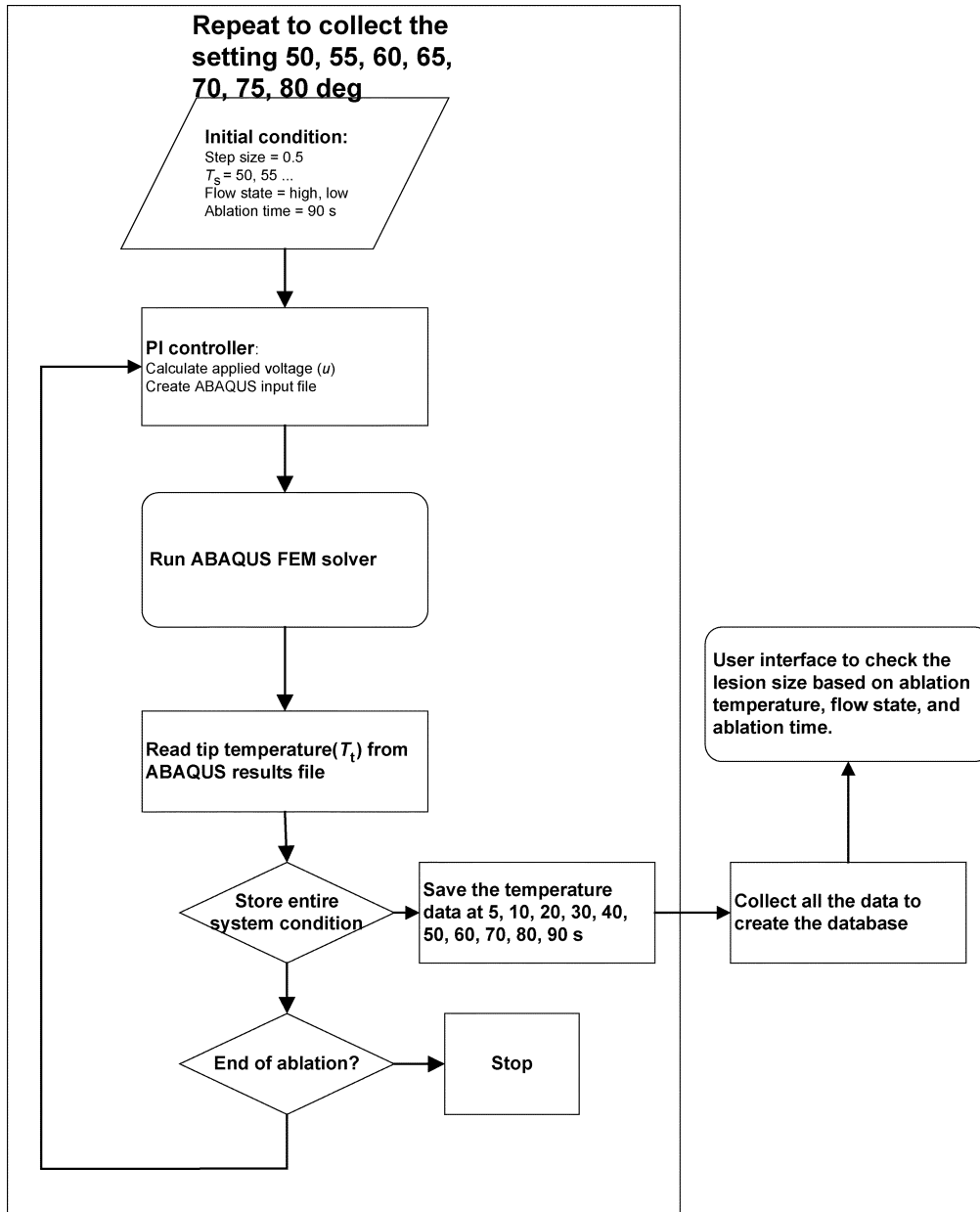


Fig. 3. The PI controller adjusts the applied voltage to maintain the tip temperature constant.

still and, thus, the convection due to fluid flow was negligible. The only heat transfer in this region was thermal conduction. We set the temperature of the blood on the boundary of the model to 37 °C, the blood temperature in the cardiac chamber. Using the Dirichlet boundary conditions, we assumed that the voltages on the outer surfaces of the model were 0 V. We determined the materials used in [12] and determined their electrical and thermal properties. The electrical conductivity of the myocardium varies +2%/°C [13]. We measured the electrical con-

ductivity at 37 °C and incremented it +2%/°C. We used the temperature-dependent thermal conductivity and the specific heat of the myocardium from Foster and Schwan [13] and Bhavaraju and Valvano [14]. Fig. 2 shows the geometry of the ablation electrode model consisting of 2799 nodes.

The cooling effect of blood depends on the location in the cardiac chambers. There are several common locations where electrophysiologists apply ablation, such as the AV node, AV valve annulus, and right

ventricular outflow tract. We divided these locations into two blood flow states. One is the high blood flow state (3 L/min) such as the AV node, and the other is the low blood flow state (1 L/min) beneath the mitral valve. The flow state was modeled by the convective heat transfer coefficients. The values of the  $h_b$  at the blood-myocardium and at the blood-electrode interfaces are different. We used  $h_b$  for the blood-myocardium interfaces from Tangwongsan *et al.* [15], who measured the *in vivo* convective heat transfer coefficients by directly inserting the measurement catheter into the pig. At the blood-electrode interface, we chose convective heat transfer coefficients which Tungjitkusolmun *et al.* [8] derived from the blood velocity measured by Ultrasound Doppler [16]. Table I lists the convective heat transfer coefficients for different blood flow at the blood-myocardium interface and the blood-electrode interface used in this study.

We used a PI controller similar to that implemented for hepatic ablation developed by Haemmerich *et al.* [9]. By analyzing the cardiac ablation system, we set the PI control coefficient to be  $K_p = 0.5$  and  $K_i = 0.3$  to minimize overshoot of the controlled temperature. The PI controller was implemented by a C++ program. The controller determined the applied voltage at each uniform step time (0.5 s) by comparing the set temperature and the temperature at the thermistor. The thermistor temperature was read from the resulting file created by ABAQUS when it finished the simulation of each time step.

### III. RESULT AND DISCUSSION

#### A. Data Collection and Lesion Size Measurement

Fig. 3 shows the entire data collection process by using our PI controller and the ABAQUS FEM solver. We ran the left part for two different blood flows and different applied temperatures. We simulated temperature-controlled ablation at temperatures of 50 °C, 55 °C, 60 °C, 65 °C, 70 °C, 75 °C, and 80 °C in different blood flow states. We acquired the temperature distribution at 10, 20, 30, 40, 50, 60, 70, 80, and 90 s after start of the ablation simulation for each set temperature.

Nath *et al.* [17] observed that when the tissue temperature reaches 50 °C, irreversible myocardial injury occurs during RF cardiac ablation. The cells lose electrical excitability and the re-entrant pathways are interrupted. Thus, 50 °C is usually considered as the threshold for lesion formation. We implemented a C++ program to search the temperature distribution in the system to find those points exceeding the critical temperature of 50 °C. Fig. 4 shows a typical shape of the lesion formed by RF ablation.  $W$  is the maximum width of the lesion, and  $D$  is the maximum depth of the lesion. The user interface estimates the  $W$  and  $D$  values from the temperature distribution.

The results are shown in Figs. 5–8. The width of the lesion increased rapidly at the beginning of the ablation and then reached a plateau for the high flow state at 30 s, and the low flow state at 40 s. The depth also grew rapidly at the beginning, and then gradually in the middle of simulation until it penetrated the entire depth of the cardiac tissue. The slope of the high flow state was higher than that of the low flow state.

#### B. Comparison to the Commercial Control Algorithm

In this simulation, we implemented the PI controller to increase the applied power monotonically at the beginning of the ablation. When the temperature approached the target temperature, the applied power decreased to maintain the monitored temperature at the target temperature so that it yielded minimum overshoot at the set temperature. This is similar to the commercial ablation generator. Thus, we expected to obtain similar temporal behavior as in the *in vivo* experiments. However, in the real commercial machine, it should monitor the temperature, power, and impedance of the tissue at the same time. Because the hot spot would not appear at the tip of the electrode, the commercial algorithm should be able to predict the temperature at the hot spot from

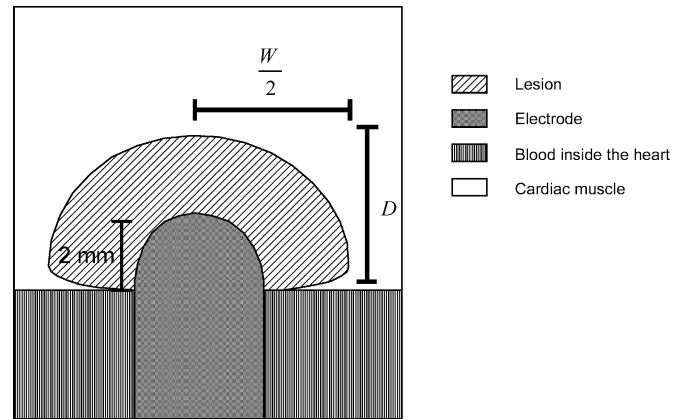


Fig. 4. Lesion volume is calculated from depth  $D$  and width  $W$ .

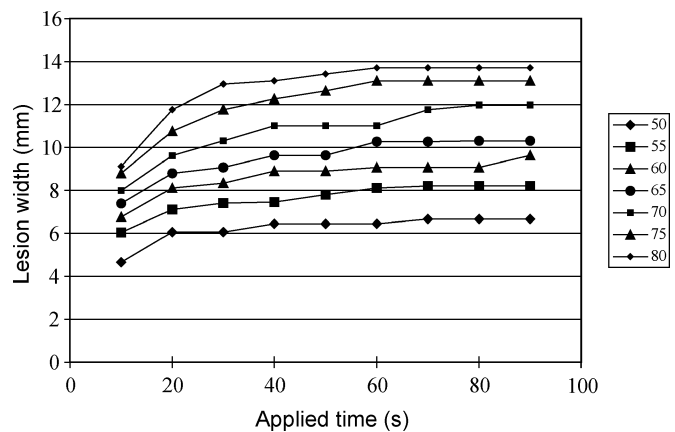


Fig. 5. Lesion width increases with ablation time at high flow.

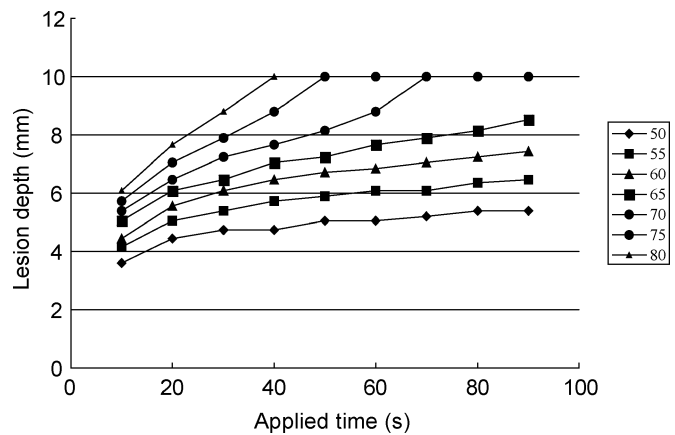


Fig. 6. Lesion depth increases with ablation time at high flow.

the temperature at the thermistor and prevent the occurrence of further injury of the myocardium such as popping. The implemented details of the machine are a commercial secret. We attempted to initiate the controlling strategy of the commercial device.

#### C. Comparison to the Results in *In Vitro* Experiments

Table II shows the comparisons of the lesion sizes between the FEM simulations and *in vitro* experiments after applying 90 s of RF ablation. First, because of the 50-W power limit in the RF generator, the highest achievable target temperature was about 73 °C at the high blood-flow region. Thus, the process at 80 °C could not achieve the expected result.

TABLE II  
COMPARISONS BETWEEN FINAL ABLATION RESULT IN FEM SIMULATIONS AND IN *INVITRO* EXPERIMENTS

Target Temperature	Blood flow	Width (mm)		Depth (mm)	
		FEM	<i>In vitro</i>	FEM	<i>In vitro</i>
60	High	9.6	10.54	7.4	5.92
	Low	8.2	7.61	6.45	3.9
70	High	11.98	12.38	10	7.14
	Low	10.3	9.96	8.09	5.3
80	High	13.7	13.63	10	7.67
	Low	12.6	11.65	10	6.45

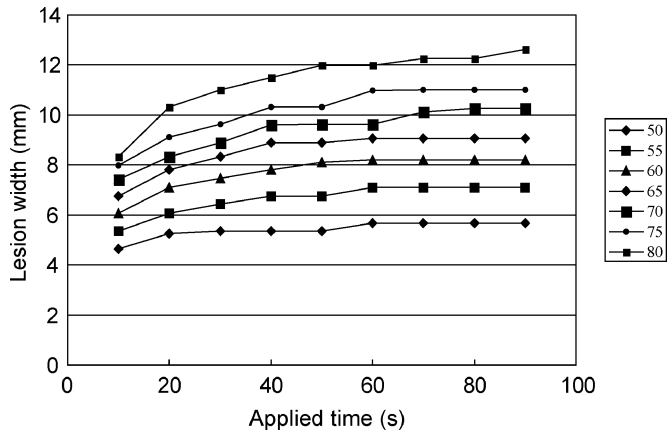


Fig. 7. Lesion width increases with ablation time at low flow.

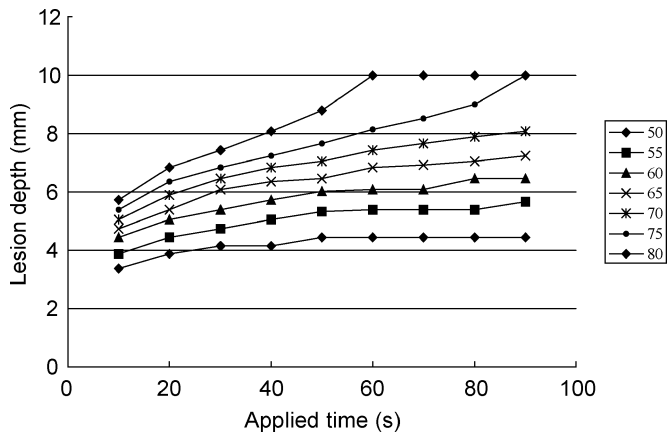


Fig. 8. Lesion depth increases with ablation time at low flow.

Second, the predictions in lesion width by FEM simulations were almost the same as the experimental results for lesion width. Third, there were prediction errors in lesion depth between simulation and experimental results, but the prediction errors were fixed at about 2.5 mm for all cases. These differences may have resulted from the catheter-myocardium contact conditions such as insertion depth, insertion angle, and deformation due to the catheter insertion.

IV. CONCLUSION

Previously published papers described the effect of the ablation time [6], tip temperature [6], control algorithm [9], and blood flow effect [8] separately. However, when electrophysiologists want to apply RF ablation to a patient, they must estimate the lesion size by considering all the variables that will affect the result. In addition, none of these papers presented the relation between applied time and the formation

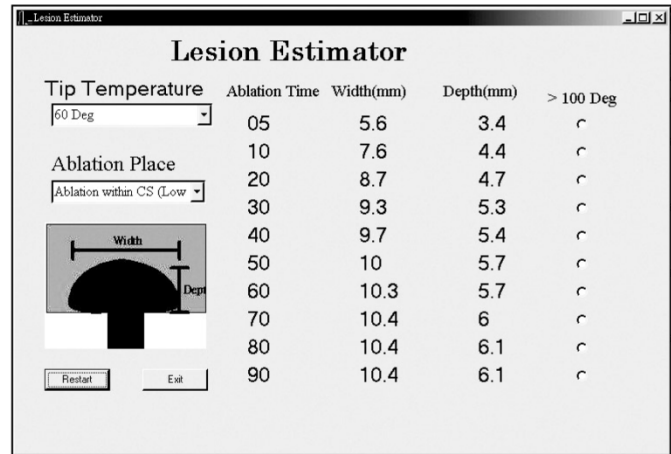


Fig. 9. A screenshot of the user interface.

of lesions. We created the preliminary architecture of software where the user can enter set temperature, ablation time and ablation location. The software shows estimates of the lesion dimensions to the user. It could be used as a first-step predictor to estimate the possible lesion formation in different settings. Fig. 9 shows a screenshot of the user interface.

However, we only used two convective heat transfer coefficients to model the different applied locations and have assumed contact of 2-mm penetration in the cardiac model during the simulation. In real life, the situation is not so simple. Thus, the following may be limitations to the precision of estimation.

- 1) In real life, the variation of the contact has a quantitative effect on the formation of the lesion. Modeling different penetration depths and angles would improve the precision.
- 2) The cardiac properties and convective heat transfer coefficients used were derived from swine myocardium. The model yielded a quantitative overview of the lesion size from the simulation, but collecting improved properties from the human heart would improve the precision of estimation.
- 3) Although blood flow in the cardiac chamber is very complex and varies from 5 L/min to almost 0 L/min, we simply divided the applied locations into high blood flow (3 L/min) and low blood flow (1 L/min). With improved knowledge of blood flow at each location, we could obtain an improved estimation of the formation of the lesion.
- 4) We used a control program that improved efficiency without human interaction during the simulation. The accuracy of the control method could be improved by determining the dynamic response of the increased tissue temperature to applied voltage during *in vivo* experiments. With information about the control methods used in the commercial generators, we could more precisely simulate process of RF ablation in the operating room.

## REFERENCES

- [1] S. K. S. Huang and D. J. Wilber, Eds., *Radiofrequency Catheter Ablation of Cardiac Arrhythmias: Basic Concepts and Clinical Applications*, 2nd ed. Armonk, NY: Futura, 2000.
- [2] D. P. Zipes and M. Haïssaguerre, *Catheter Ablation of Arrhythmias*, 2nd ed. Armonk, NY: Futura, 2002.
- [3] F. Morady, "Drug therapy: Radio-frequency ablation as treatment for cardiac arrhythmias," *N. Eng. J. Med.*, vol. 340, pp. 534–544, 1999.
- [4] D. Panescu, "Intraventricular electrogram mapping and radiofrequency cardiac ablation for ventricular tachycardia," *Physiol. Meas.*, vol. 18, pp. 1–38, 1997.
- [5] H. Nakagawa, K. J. Beckman, and J. H. McClelland, "Radiofrequency catheter ablation of idiopathic left ventricular tachycardia guided by a Purkinje potential," *Circulation*, vol. 85, pp. 1666–1674, 1992.
- [6] S. Tungjitkusolmun, E. J. Woo, H. Cao, J.-Z. Tsai, V. R. Vorperian, and J. G. Webster, "Thermal-electrical finite element modeling for radio-frequency cardiac ablation: Effects of changes in myocardial properties," *Med. Biol. Eng. Comput.*, vol. 38, pp. 562–568, 2000.
- [7] H. Cao, V. R. Vorperian, S. Tungjitkusolmun, J.-Z. Tsai, D. Haemmerich, Y. B. Choy, and J. G. Webster, "Flow effect on lesion formation in RF cardiac catheter ablation," *IEEE Trans. Biomed. Eng.*, vol. 48, pp. 425–433, Apr. 2001.
- [8] S. Tungjitkusolmun, V. R. Vorperian, N. Bhavaraju, H. Cao, J.-Z. Tsai, and J. G. Webster, "Guidelines for predicting lesion size at common endocardial locations during radio-frequency ablation," *IEEE Trans. Biomed. Eng.*, vol. 48, pp. 194–201, Feb. 2001.
- [9] D. G. Haemmerich, "Finite element modeling of hepatic radio-frequency ablation," Ph.D. dissertation, Univ. Wisconsin-Madison, Madison, WI, 2001.
- [10] D. Panescu, J. G. Wayne, S. D. Fleischman, M. S. Mirotznik, D. K. Swanson, and J. G. Webster, "Three-dimensional finite element analysis of current density and temperature distributions during radio-frequency ablation," *IEEE Trans. Biomed. Eng.*, vol. 42, pp. 879–890, Sept. 1995.
- [11] H. H. Peterson, X. Chen, A. Pietersen, J. H. Svendsen, and S. Hauns, "Lesion dimensions during temperature-controlled radiofrequency catheter ablation of left ventricular porcine myocardium: Impact of ablation size, electrode size and convective cooling," *Circulation*, vol. 99, pp. 319–325, 1999.
- [12] S. D. Edwards and R. A. Stern, "Electrode and Associated Systems Using Thermally Insulated Temperature Sensing Elements," U. S. Patent 5 688 266, 1997.
- [13] K. R. Foster and H. P. Schwan, "Dielectric properties of tissues and biological materials: A critical review," *CRC Crit. Rev. Biomed. Eng.*, vol. 17, pp. 25–104, 1989.
- [14] N. C. Bhavaraju and J. W. Valvano, "Thermophysical properties of swine myocardium," *Int. J. Thermophys.*, vol. 20, pp. 665–676, 1999.
- [15] C. Tangwongsan, J. A. Will, J. G. Webster, K. L. Meredith Jr., and D. M. Mahvi, "In vivo measurement of swine endocardial convective heat transfer coefficient," *IEEE Trans. Biomed. Eng.*, vol. 51, pp. 1478–1486, Aug. 2004.
- [16] A. B. Houston and I. A. Simpson, Eds., *Cardiac Doppler Ultrasound: A Clinical Perspective*. Boston, MA: Wright, 1988.
- [17] S. Nath, C. Lynch, J. G. Wayne, and D. E. Haines, "Cellular electrophysiological effects of hyperthermia on isolated guinea pig papillary muscle implication for catheter ablation," *Circulation*, pt. 1, vol. 88, pp. 1826–1831, 1993.